Supporting information

for

Lighting Up Aggregate Emission of Perylene Diimide by Leveraging Polymerization-Mediated Through-Space Charge Transfer and π-π Stacking

Suiying Ye[1], Désirée Füglistaller[1], Tian Tian[2], Anjay Manian[3], Sudhir Kumar[2], Celine Nardo[1], Andrew J. Christofferson[3,4], Salvy P. Russo[3], Chih-Jen Shih[2], Jean-Christophe Leroux[1], Yinyin Bao[*, 1]

[1]Institute of Pharmaceutical Sciences, Department of Chemistry and Applied Biosciences, ETH Zurich, Vladimir-Prelog-Weg 3, 8093 Zurich, Switzerland.

[2] Institute for Chemical and Bioengineering, Department of Chemistry and Applied Biosciences, ETH Zurich, Vladimir-Prelog-Weg 1-5/10, 8093 Zurich, Switzerland.

[3] ARC Centre of Excellence in Exciton Science, School of Science, RMIT University, Melbourne, Victoria, 3001, Australia

[4]School of Science, STEM College, RMIT University, Melbourne, Victoria 3001, Australia.

[*]Corresponding author. Email: ybao@ethz.ch

Materials

Unless stated otherwise, all reagents were used as received without further purification. N,N-Dimethylformamide (DMF, 99.8%, extra dry over molecular sieve), pyridine (99.5%, extra-dry over molecular sieves), tetrahydrofuran (THF, 99.5%, extra-dry over molecular sieve), toluene (99.5%, extra-dry over molecular sieve), dichloromethane (DCM, ≥99.8%), 1,4-dioxane (99.5% extra-dry over molecular sieve), styrene (St, 99.5%), 2-vinylnaphthalene (2VN, 98%), 1,1,4,7,7-pentamethyldiethylenetriamine (PMDETA, 99+%), and 3-aminopropane-1,2-diol (98%) were purchased from Acros Organics (Fair Lawn, NJ, USA). Copper(I) bromide (CuBr, 99.998% metals basis) and perylene-3,4,9,10-tetracarboxylic acid dianhydride (98%), and benzyl methacrylate (BMA, 98%) were obtained from Alfa Aesar (Haverhill, MA, USA). Methyl methacrylate (MMA, >99.8%, GC) and 4,4'-dinonyl-2,2'-bipyridyl (dNbpy, >98.0%) were obtained from TCI (Tokyo, Japan). Methanol (gradient grade ≥99.9%), mesitylene (98%), benzene anhydrous (99.8%), N,N-dimethylacetamide (≥99.9%), aluminum oxide basic, 2-aminoethanol (≥99.0%), α-bromoisobutyryl bromide (BIBB, 98%), 1-pyrenemethyl methacrylate (PyMA, 99%), 9-fluorenyl methacrylate (FluoMA, 97%), hexane (≥97%), anisole (99%), and silica gel 60 (for chromatography) were purchased from Sigma Aldrich (St. Louis, MO, USA). Tetrahydrofuran (THF, >99.5%), xylenes (mixture of isomers, >96.0%), and toluene (>99.5%) were purchased from VWR International (Radnor, PA, USA). Ethanol absolute (>99.8%) and DMF (laboratory reagent grade) were obtained from Fisher Scientific (Loughborough, UK). Acetone-d6 (99.9% deuterated) and chloroform-d ($CDCl_3$, 99.8% deuterated) were acquired from Cambridge Isotope Laboratories Inc. (Tewksbury, MA, USA). 1-Vinylpyrene (VPy, 95%), 9-anthracenylmethyl methacrylate (AntMA, 95%), and 2-(methacryloyloxy)ethyl anthracene-9-carboxylate (AntMAc, 95%) were obtained from Career Henan Chemical Co. (Henan, China). Dichloromethane-d2 (CD_2Cl_2, 99.5% deuterated) was obtained from Chemie Brunschwig (Basel, Switzerland).

Measurements

Single crystalline samples were measured on a Rigaku Oxford Diffraction XtaLAB Synergy-S Dualflex kappa diffractometer (Tokyo, Japan) equipped with a Dectris Pilatus 300 HPAD detector and using microfocus sealed tube Cu-Kα radiation with mirror optics (λ = 1.54178 Å). All measurements were carried out at 100 K (unless noted otherwise) using an Oxford Cryosystems Cryostream 800 (Oxford, UK) sample cryostat. Data were integrated using CrysAlisPro and corrected for absorption effects using a combination of empirical (CrysAlisPro and ABSPACK. Rigaku Oxford Diffraction, 2016) and numerical corrections. The structures were solved using SHELXT[1] and refined by full-matrix least-squares analysis (SHELXL)[2], using the program package OLEX2[3]. Unless otherwise indicated below, all non-hydrogen atoms were refined anisotropically, and hydrogen atoms were constrained to ideal geometries and refined with fixed isotropic displacement parameters (in terms of a riding model). CCDC 2322608 (DOI: 10.5517/ccdc.csd.cc2hyvv5) contains the supplementary crystallographic data for this paper, including structure factors and refinement instructions. These data can be obtained free of charge from The Cambridge Crystallographic Data Centre, 12 Union Road, Cambridge CB2 1EZ, UK (fax: +44(1223)-336-033; e-mail: deposit@ccdc.cam.ac.uk), or via https://www.ccdc.cam.ac.uk/getstructures.

Powder X-ray diffraction was done with a Panalytical X'PERT-PRO MPD diffractometer (Almelo, Netherlands) with Bragg-Brentano geometry (scan-range 2° - 90°, step-width 0.0167°, Cu-Kα1 radiation).

Proton Nuclear Magnetic Resonance (^{1}H NMR) spectra were recorded on an AV-400 400 MHz spectrometer (Bruker, Billerica, MA, USA) at room temperature. Gel permeation chromatography (GPC) measurements were carried out on a system from Shimadzu (Kyoto, Japan), including a CBM-20A system controller, a SIL-20A HT auto 14 sampler, a guard column (50 × 7.5 mm, bead size: 10.0 μm) followed by three KF-805L columns (300 × 8 mm, bead size: 10 μm, pore size maximum: 5000 Å), an SPD-20A ultraviolet detector, and a RID-20A refractive-index detector. Measurements were conducted at 40 °C using a CTO-20A oven. N,N-Dimethylacetamide (with 0.03% LiBr) was used as eluent at a flow rate of 1 mL min^{-1} using an LC-20AD pump. Commercial, narrow molecular weight distribution poly(methyl methacrylate) with molecular weights ranging from 5000 to 1.5×10^6 g mol^{-1} were used as standards. Samples were prepared at a concentration of 1 mg mL^{-1} and filtered through PTFE membrane filters (0.45 μm pore size) before injection. Dynamic light scattering measurements on PDI polymers in DMF/H_2O mixtures were performed on a Zetasazier Nano (Malvern Instruments) with literature values of viscosity, refractive index, and dielectric constants of different DMF/H_2O mixtures.[4,5]

UV-Vis absorption spectra for samples in thin films were obtained with Agilent Cary 60 spectrophotometer (Santa Clara, CA, USA). UV-Vis absorption spectra for samples in suspensions were recorded with TECAN Infinite M200 PRO Multimode Microplate (Zurich, Switzerland). Photoluminescence (PL) spectra of samples in solutions/suspensions were obtained with a Cary Eclipse fluorescence spectrophotometer. PL spectra of thin film samples and time-resolved photoluminescence (TRPL) traces were characterized using a Hamamatsu Quantaurus-Tau Fluorescence Lifetime Spectrometer (C11367-31) equipped with a photon counting measurement system. The TRPL samples were excited using a 365-nm pulsed emission with a repetition rate of 100 kHz and 10000 counts. The absolute photoluminescence quantum yields (PLQYs) of powders and spin-casted thin films were determined using the Quantaurus QY (C11347-11) from Hamamatsu equipped with 150W xenon light source and a 3.3-inch (8.38 cm) integrating sphere, which is coated with highly reflective Spectralon. For thin films produced with polymers, a typical spin-casting method was applied with toluene as the solvent. In specific, glass substrates with a size of 10 × 10 mm were brush-cleaned using the mixture of Extran MA02 soap solution and water (1:3, v/v). Subsequently, all substrates were sonicated in acetone and isopropanol, respectively. These substrates were then dried on a hot plate at 120 ºC for 20 min. Finally, the sample solutions were spin-casted at a spin rate of 2000 rpm for 50 s.

Table S1. Photophysical properties of PDI homopolymers.

Product	DP_{NMR}	$M_{n,\,NMR}$ *(g.mol^{-1})*	$M_{n,\,GPC}$ *(g.mol^{-1})*	$Đ$	$\lambda_{em,\,film}$	Φ_{film}
PDI-diPS	19	2760	2460	1.09	645	12.07 (0.058)
	27	3590	3130	1.13	646	22.13 (0.058)
	41	5050	3850	1.13	641	25.97 (0.058)
	62	7230	5830	1.16	635	31.70 (0.100)
	89	10050	6720	1.23	640	35.10 (0.200)
PDI-tetraPS	15	2700	2600	1.14	656	12.70 (0.100)
	20	3220	2750	1.11	642	20.80 (0.100)
	30	4260	3290	1.12	641	23.20 (0.100)
	40	5300	4130	1.13	640	26.67 (0.208)
	62	7590	5320	1.13	636	33.27 (0.262)
	71	8530	6210	1.14	631	39.13 (0.577)
	80	9470	7620	1.09	630	43.03 (0.208)
	100	11550	7550	1.14	628	44.90 (0.100)
PDI-diPMMA	29	3680	4100	1.53	654	19.87 (0.058)
	52	5980	7070	1.50	649	24.90 (0.100)
	76	8390	12590	1.69	646	25.13 (0.058)
	112	11990	15910	1.48	640	30.20 (0.265)
PDI-tetraPMMA	23	3440	5310	1.51	648	22.27 (0.231)
	38	4940	7620	1.78	647	24.90 (0.100)
	58	6940	8430	1.52	636	29.53 (0.058)
	79	9040	11250	1.55	633	31.60 (0.173)
	95	10650	22290	1.49	628	35.73 (0.058)
PDI-tetraPBMA	28	6070	6830	1.57	637	28.07 (0.115)
	52	10300	11980	1.66	629	36.50 (0.361)
	79	15060	15040	1.51	625	37.03 (0.473)
	103	19290	22070	1.52	621	37.47 (0.462)

Table S2. Exciton lifetime of PDI homopolymers.

Product	DP_{NMR}	χ	τ_{avg}	t_1	t_2
PDI-diPS	62	1.03	25.24	11.37	28.43
PDI-tetraPS	20	1	18.74	7.93	21.64
	62	1.01	22.38	6.52	25.8
	100	1.11	25.99	9.32	28.89
PDI-diPMMA	52	0.98	28.31	18.99	34.62
PDI-tetraPMMA	58	1.01	31.64	12.28	35.2
PDI-tetraPBMA	52	1.04	32.54	10.76	35.13

Table S3. Photophysical properties of PDI polymers containing PAMs.

Product	[St]/[PAM]/[I]	PAM feed	$DP_{St, NMR}$	$DP_{PAM, NMR}$	PAM load	$M_{n, NMR}$ (g mol^{-1})	$M_{n, GPC}$ (g mol^{-1})	$Đ$	$\lambda_{em, film}$ (nm)	Φ_{film} (%)
PDI-poly2VN	0/80/1	-	-	25	-	4990	2730	1.08	658	15.10 (0.002)
PDI-*co*2VN	79.2/0.8/1	1%	55	0.49	0.9%	6940	5780	1.15	634	34.70 (0.001)
	76/4/1	5%	44	1.89	4.1%	6010	4880	1.12	636	31.13 (0.001)
	72/8/1	10%	47	4.26	8.3%	6690	4710	1.12	640	29.23 (0.002)
	64/16/1	20%	29.6	5.85	16.5%	5120	3740	1.1	642	29.27 (0.002)
PDI-*co*FluoMA	79.2/0.8/1	1%	67	0.17	0.3%	8160	5510	1.14	634	31.97 (0.002)
	76/4/1	5%	26	0.76	2.8%	4030	3260	1.11	649	25.50 (0.001)
	72/8/1	10%	26	1.45	5.3%	4210	3380	1.11	651	26.57 (0.001)
	68/12/1	15.00%	17.75	2.65	13.0%	3650	2870	1.1	653	23.73 (0.002)
PDI-*co*AntMAc	156/4/1	2.5%	18.8	1.40	6.9%	3560	5170	1.77	666	14.30 (0.001)
	144/16/1	10.0%	15	2.09	12.2%	3400	4970	1.68	670	11.97 (0.002)
	136/24/1	15.0%	18	4.00	18.2%	4350	5150	1.73	677	10.87 (0.002)
	112/48/1	30.0%	3.5	3.60	50.7%	2700	4920	1.41	680	9.00 (0.002)
PDI-*co*AntMA	156/4/1	2.5%	48.3	2.00	4.0%	6720	5080	1.68	683	7.10 (0.002)
	144/16/1	10.0%	19.6	2.24	10.3%	3790	3590	1.37	693	5.23 (0.001)
	136/24/1	15.0%	19.9	8.50	29.9%	5560	4140	1.58	707	4.00 (0.000)
	112/48/1	30.0%	21.1	10.80	33.9%	6320	4240	1.45	714	3.83 (0.002)
PDI-*co*PyMA	79.2/0.8/1	1%	37.5	0.33	0.9%	5140	3650	1.11	673	14.07 (0.002)
	76/4/1	5%	28	1.60	5.4%	4530	2950	1.09	695	6.40 (0.001)
	72/8/1	10%	17.2	3.80	18.1%	4070	2520	1.07	716	2.10 (0.001)
	68/12/1	15%	21.3	6.08	22.2%	5180	2800	1.08	718	3.50 (0.001)
PDI-*co*VPy	79.6/0.4/1	0.50%	61.6	0.30	0.5%	7620	4890	1.15	678	7.57 (0.001)
	79.4/0.6/1	0.75%	56.91	0.74	1.3%	7230	4560	1.15	691	5.23 (0.000)
	79.2/0.8/1	1%	44.54	0.89	2.0%	5980	3660	1.14	710	3.42 (0.000)
	78/2/1	2.50%	24	3.45	12.6%	4420	2590	1.14	744	1.83 (0.001)
	76/4/1	5%	22	7.00	24.1%	5020	-	-	-	1.23 (0.001)

Table S4. Exciton lifetime of PDI polymers containing PAMs.

Product	PAM feed	χ	τ_{avg}	t_1	t_2
PDI-poly2VN	100%	1.01	17.13	8.84	22.54
PDI-*co*2VN	20%	0.95	21.659	7.66	24.38
PDI-*co*FluoMA	15%	0.98	21.36	6.84	24.1
PDI-*co*AntMAc	30%	1.02	10.92	5.52	12.65
PDI-*co*AntMA	30%	0.95	7.86	4.99	9.16
PDI-*co*PyMA	15%	0.98	7.71	5.53	10.67
PDI-*co*VPy	5%	1.06	6.79	4.5	13.58

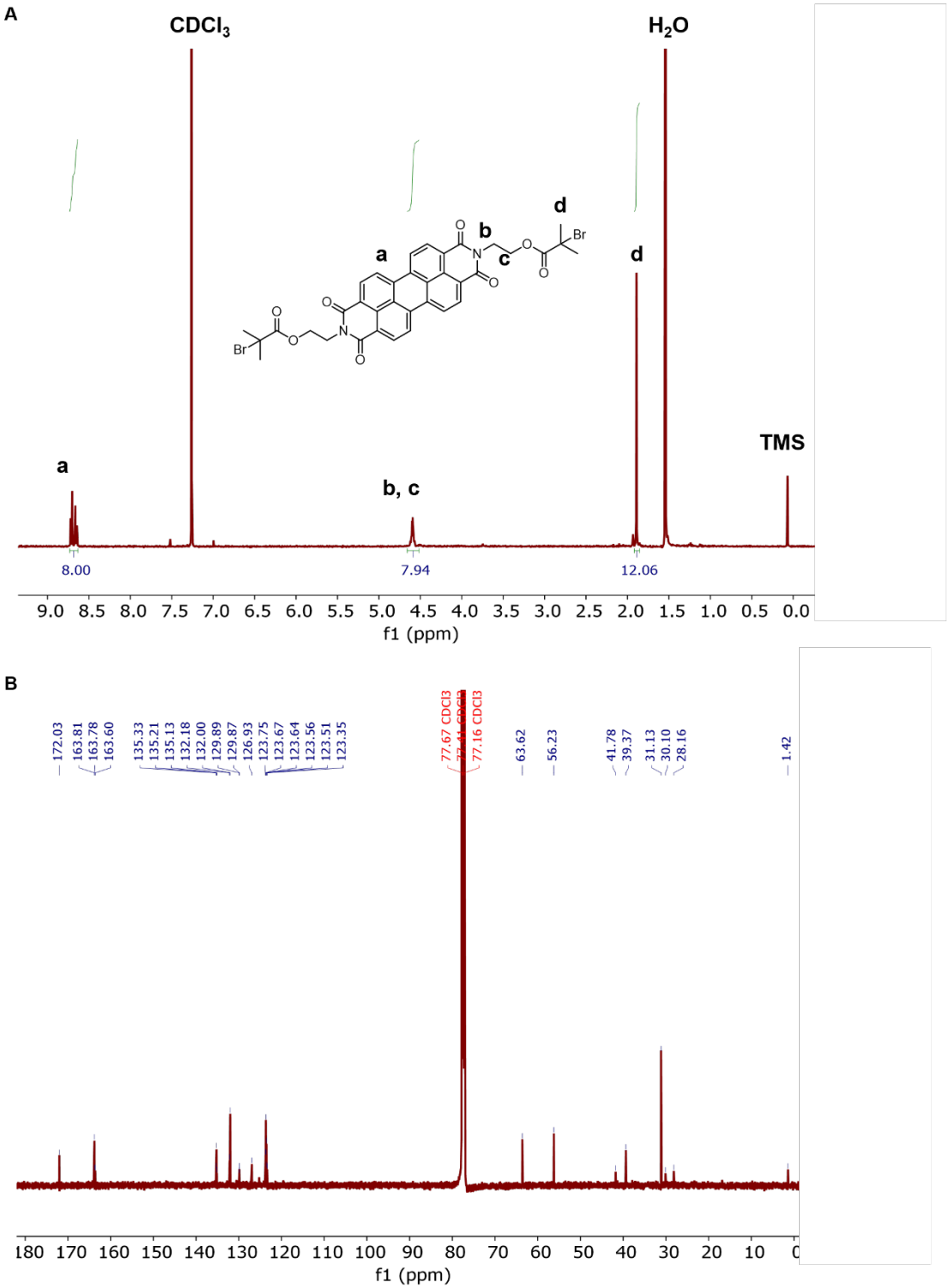

Figure S1. Structure characterization of PDI-diBr. (A) ^{1}H NMR and (B) ^{13}C NMR spectra of PDI-diBr in $CDCl_3$.

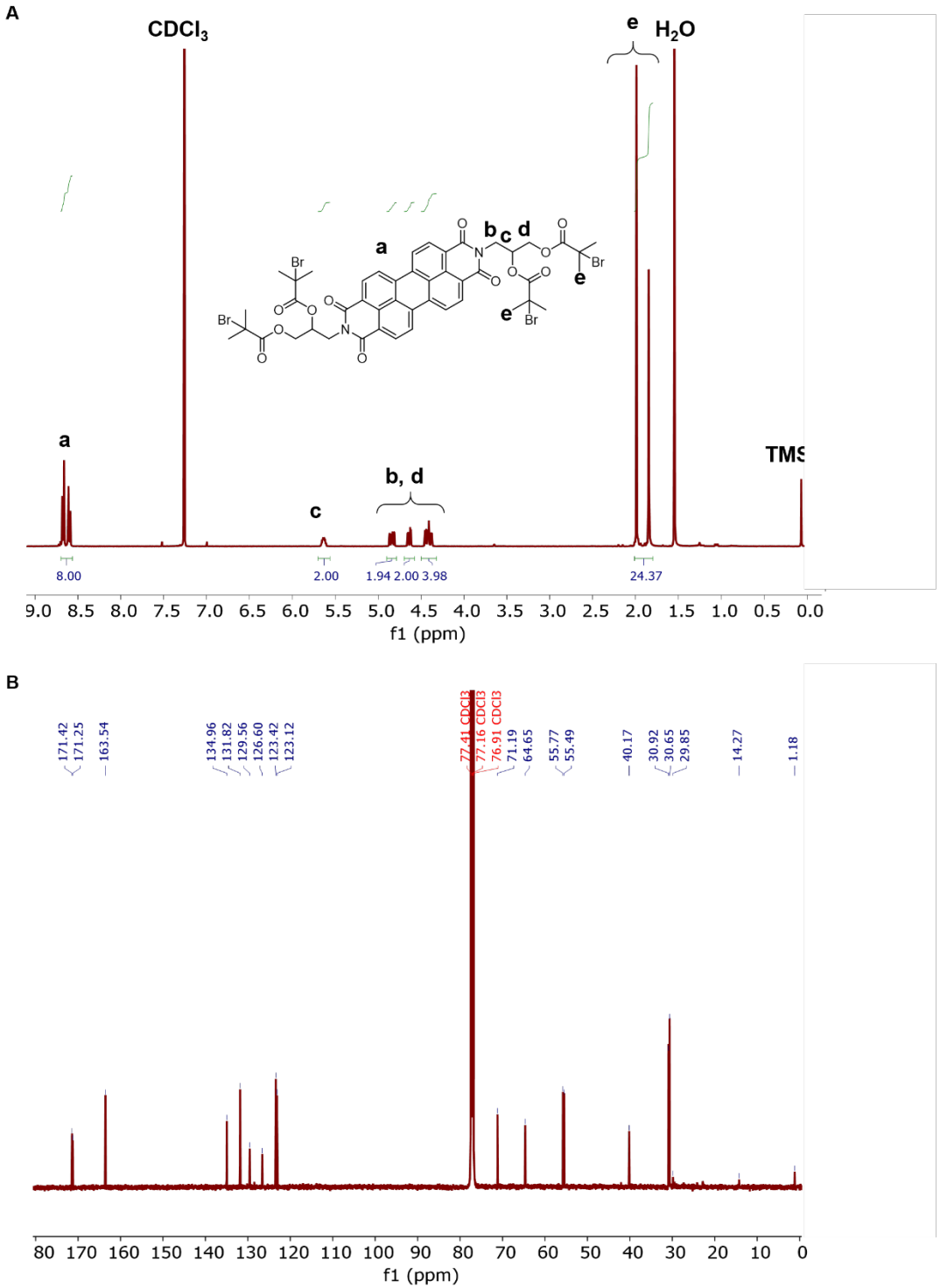

Figure S2. Structure characterization of PDI-tetraBr. (A) ^{1}H NMR and (B) ^{13}C NMR spectra of PDI-tetraBr in $CDCl_3$.

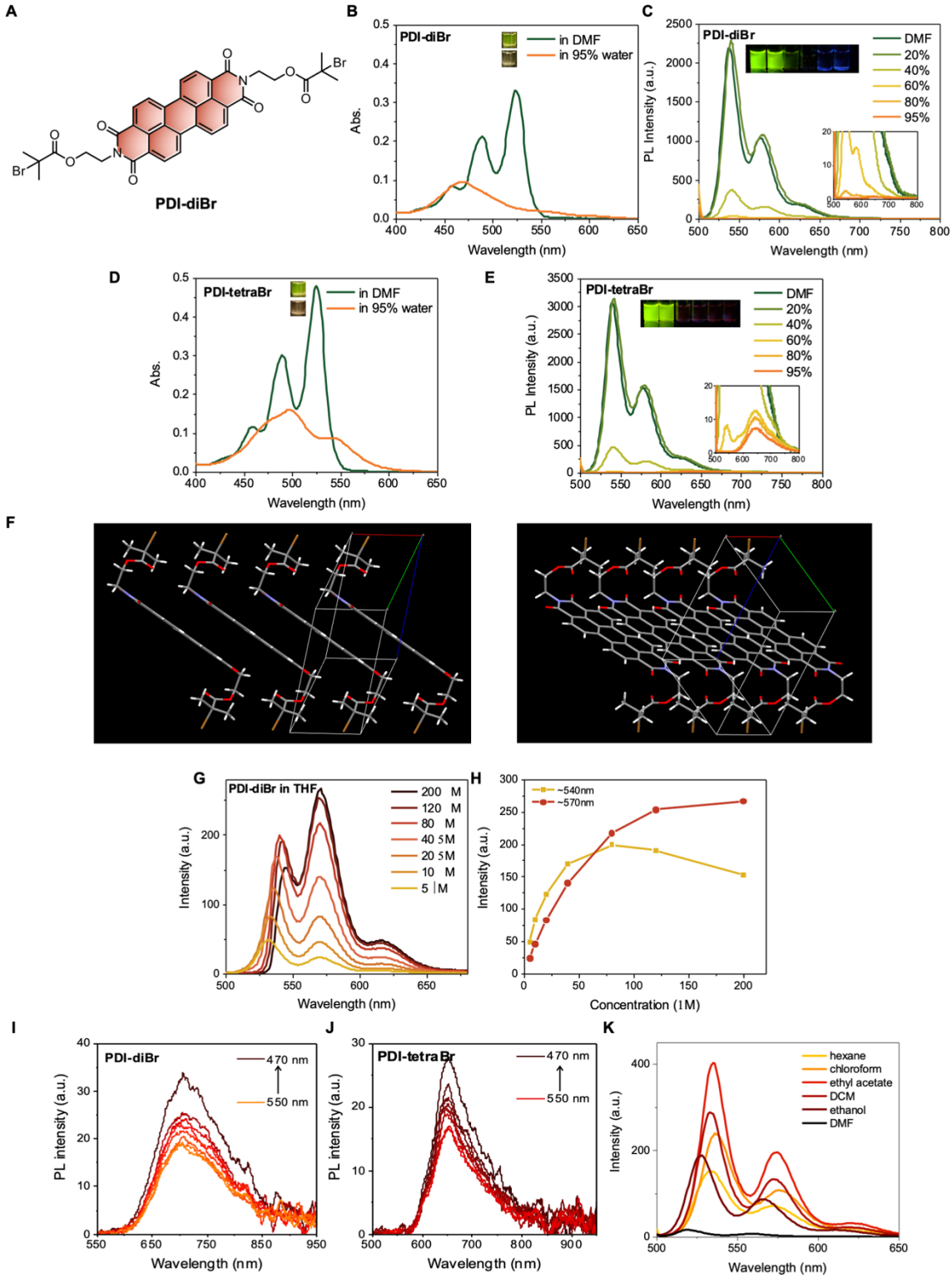

Figure S3. Crystal structure of PDI-diBr and photophysical properties of PDI-diBr and PDI-tetraBr. (A) Chemical structure of PDI-diBr. (B-E) Absorption spectra and PL spectra of PDI-diBr (B, C, respectively) and PDI-tetraBr (D, E, respectively) in DMF or DMF/H_2O (80/20 to 5/95, v/v). Insets: Photographs of polymers in DMF or DMF/H_2O under ambient light (B, D) and 365 nm-UV (C, E). (F) Molecular packing of PDI-diBr single crystals from side and front view. (G-H) PL spectra of PDI-diBr in THF (G) and the intensity at ~540 nm and ~570 nm (H) at different concentrations. (I-J) PL spectra of PDI-diBr (I) and PDI-tetraBr (J) in powder with different excitation wavelengths. (K) PL spectra of PDI-diBr at 5.0 μM in various organic solvents.

Discussion for Figure S3

Due to the poor solubility (~0.5 mg mL^{-1} in chloroform), the synthesis yield of **PDI-diBr** (**Figure S3A**) was only ~14%. As for **PDI-tetraBr** (**Figure 2A**), it was easily obtained under mild conditions with a yield of ~46%, thanks to its much better solubility (~4 mg mL^{-1} in chloroform).

The photophysical properties of **PDI-diBr** and **PDI-tetraBr** were then characterized. When dissolved in N,N-dimethylformamide (DMF), both molecules showed three typical absorption peaks (458, 489, 525 nm), alongside a shoulder peak (~425 nm) (**Figures S3**, **B and D**, dark green curves).[6] Meanwhile, nearly mirror images of the absorption spectra were observed for the fluorescence emission of **PDI-diBr** and **PDI-tetraBr** (**Figures S3**, **C and E**, dark green curves). To evaluate their photophysical properties in an aggregate state, both initiators were dispersed in DMF/H_2O (5/95, v/v). **PDI-diBr** exhibited a broadened peak losing the vibronic structures with a clear hypsochromic shift of the absorption maxima to ~470 nm (**Figure S3**, **B**, orange curve). This feature usually originates from the co-facial aggregation of PDI (typically H-aggregation),[7,8] which was further confirmed by the single-crystal x-ray diffraction and spectrophotometry showing a π-π packing distance of 6.14 Å (**Figure S3**, **F**). On the other hand, **PDI-tetraBr** showed the absorption maximum at ~500 nm and a significant shoulder peak at ~550 nm (**Figure S3**, **D**, orange curve), in the aggregate state (DMF/H_2O 5/95, v/v). Apparently, the packing mode of **PDI-tetraBr** cannot be fully attributed to the H-type aggregate, possibly because of a rotational displacement in PDI stacking induced by the tetra-functionalized structure.[8-10] A similar observation was reported in other star-shaped PDI molecules.[9-12] The fluorescence spectra of both molecules were recorded in DMF/H_2O mixtures with increasing water fraction. Conceivably, drastic fluorescence quenching was observed for both molecules in aggregates (**Figures S3**, **C and E, orange curves**) due to the strong π-π stacking of the PDI scaffold. The stacking was also indicated by the enhanced transitions in the higher levels of electronic states (0-1 at ~570 nm, 0-2 at 620 nm) with respect to 0-0 transition (~540 nm) upon increasing molecular concentration (**Figure S3**, **G and H**).[12]

Notably, a weak red-emission peak appeared at ~650 nm for **PDI-tetraBr** with a water fraction of ⩾ 60%, which was not observed in **PDI-diBr**. In solid state, **PDI-tetraBr** showed a significant blueshift in emission compared to **PDI-diBr** (650 nm *vs.* 700 nm, **Figure S3**, **I and J**). These results again highlight the influence of the four α-bromoisobutyryl groups on the packing configuration of **PDI-tetraBr**. Unfortunately, the single crystal of **PDI-tetraBr** suitable for structure analysis could not be obtained, likely due to the high flexibility of co-existing four α-bromoisobutyryl groups. Despite that, the significant difference between **PDI-diBr** and **PDI-tetraBr** in photophysical properties drove us to investigate whether such an effect could be observed in polymer systems, where structural distortion and CT may occur simultaneously.

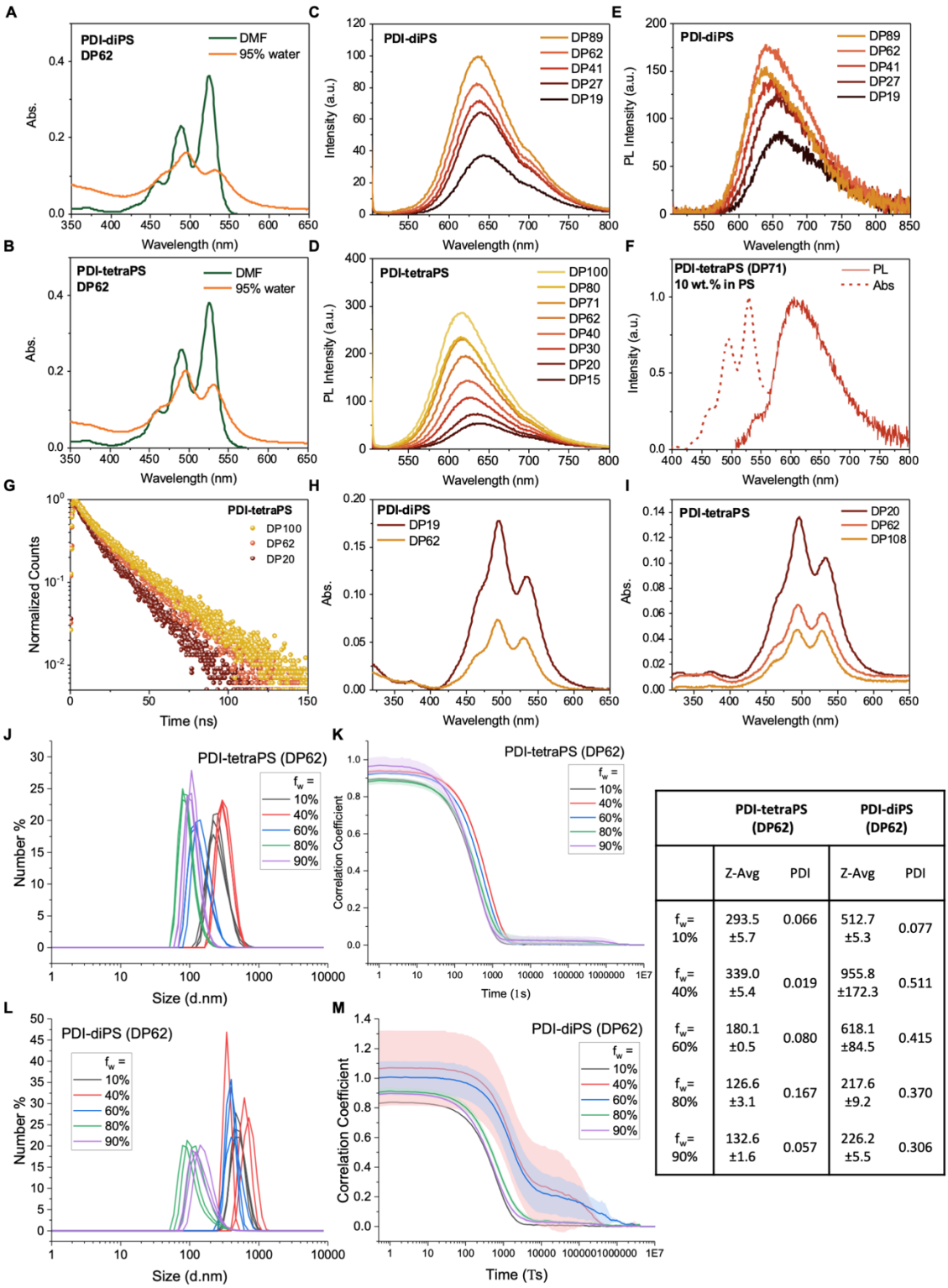

	PDI-tetraPS (DP62)		PDI-diPS (DP62)	
	Z-Avg	PDI	Z-Avg	PDI
f_w= 10%	293.5 ±5.7	0.066	512.7 ±5.3	0.077
f_w= 40%	339.0 ±5.4	0.019	955.8 ±172.3	0.511
f_w= 60%	180.1 ±0.5	0.080	618.1 ±84.5	0.415
f_w= 80%	126.6 ±3.1	0.167	217.6 ±9.2	0.370
f_w= 90%	132.6 ±1.6	0.057	226.2 ±5.5	0.306

Figure S4. PL properties of PDI-diPS and PDI-tetraPS. (A-B) Absorption spectra of PDI-diPS (DP62) and PDI-tetraPS (DP62) in DMF or DMF/H_2O (5/95, v/v). (C-D) PL spectra of PDI-diPS and PDI-tetraPS of various DP in DMF/H_2O (5/95, v/v). (E) PL spectra of solid films produced with PDI-diPS of various DP. (F) Absorption and PL sepctra of PDI-tetraPS (DP71) in a polystyrene matrix. (G) Lifetime decay profiles of solid films produced with PDI-tetraPS of various DPs. (H-I) Absorption spectra of solid films produced with PDI-diPS and PDI-tetraPS of various DPs. The concentration of the polymers was 5.0 μM. The excitation wavelength was 497 nm. (J-M) Dynamic light scattering measurements PDI-diPS (DP62) and PDI-tetraPS (DP62) 5.0 μM in DMF/H_2O at various water ratios f_w%. The measurements were performed on a Zetasazier Nano (Malvern Instruments) with literature values of viscosity, refractive index, and dielectric constants of DMF/H_2O mixtures.

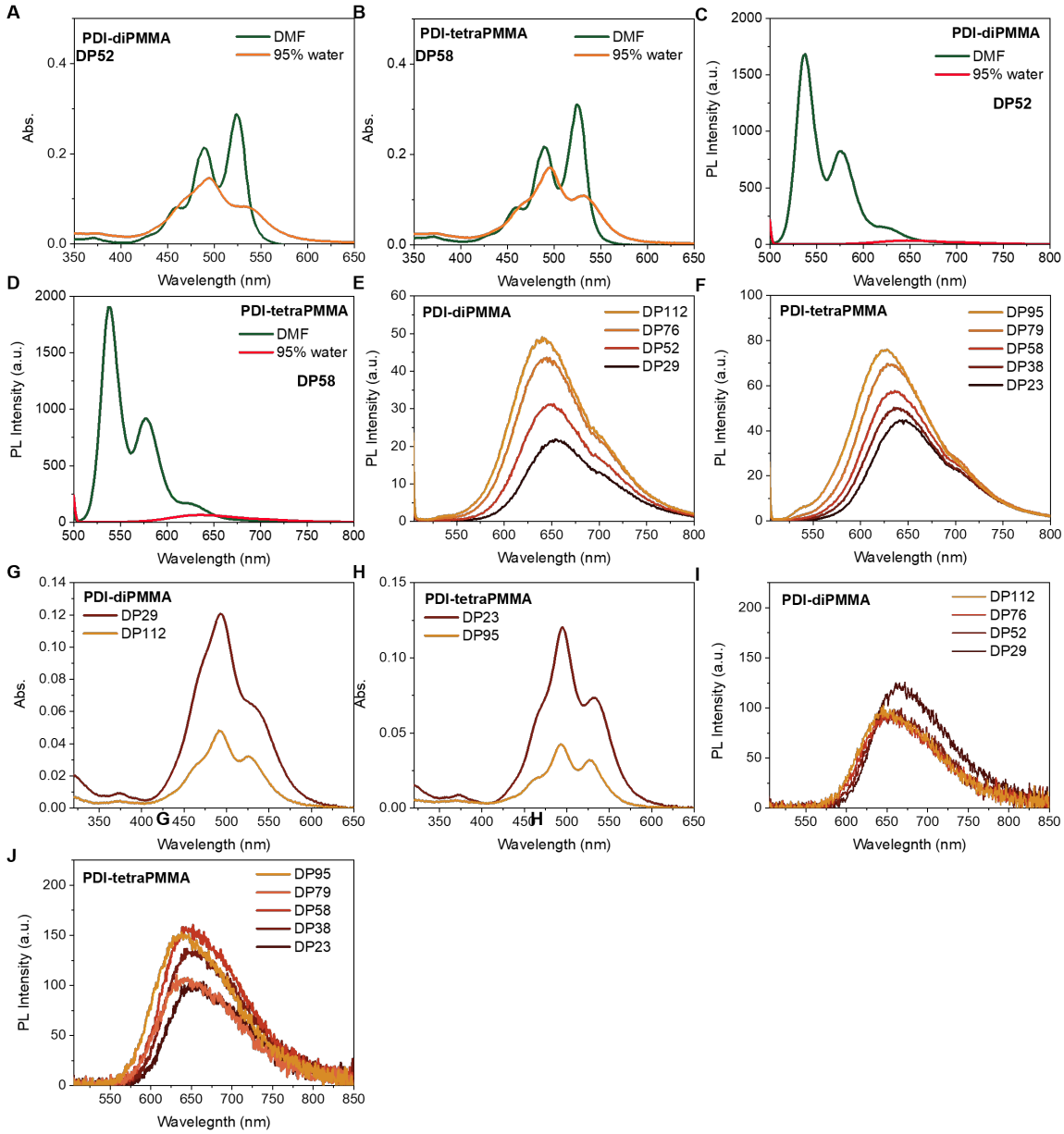

Figure S5. PL properties of PDI-diPMMA and PDI-tetraPMMA. (A-D) Absorption spectra (A and B) and PL spectra (C and D) of PDI-diPMMA (DP52) and PDI-tetraPMMA (DP58) in DMF or DMF/H_2O (5/95, v/v). (E-F) PL spectra of PDI-diPMMA and PDI-tetraPMMA of various DP in DMF/H_2O (5/95, v/v). (G-J) Absorption spectra (G and H) and PL spectra (I and J) of solid films produced with PDI-diPMMA and PDI-tetraPMMA of various DPs. The concentration of the polymers was 5.0 μM. The excitation wavelength was 497 nm.

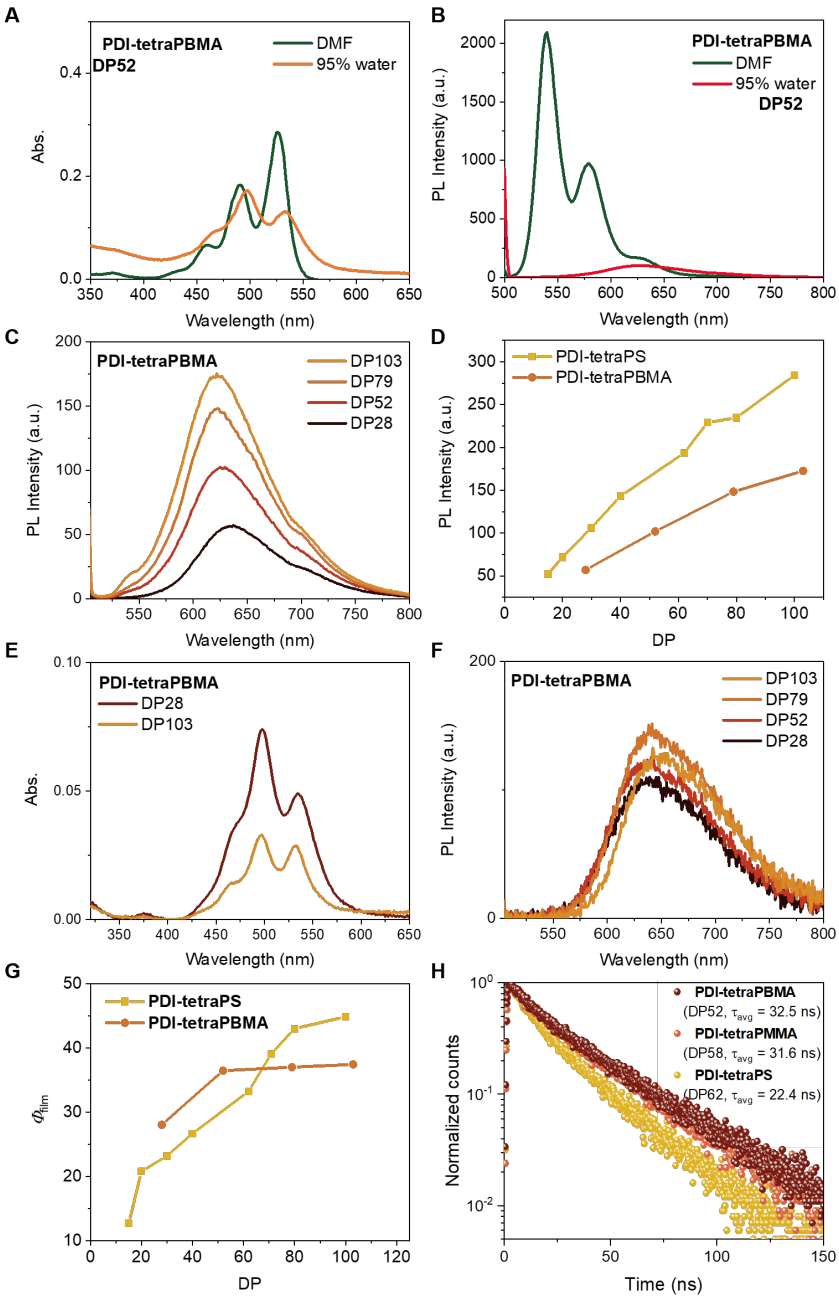

Figure S6. PL properties of PDI-tetraPBMA and the comparison with PDI-tetraPS. (A-B) Absorption spectra (A) and PL spectra (C) of PDI-tetraPBMA (DP52) in DMF or DMF/H_2O (5/95, v/v). (C) PL spectra of PDI-tetraPBMA of various DP in DMF/H_2O (5/95, v/v). (D) The comparison of peaked PL intensities in DMF/H_2O (5/95, v/v) between PDI-tetraPBMA and PDI-tetraPS at various DP. (E-F) Absorption spectra (E) and PL spectra (F) of solid films produced with PDI-tetraPBMA of various DPs. (G) The comparison of peaked PL intensities between the solid films of PDI-tetraPBMA and PDI-tetraPS at various DP. (H) Lifetime decay profiles of solid films produced with PDI-tetraPS (DP62), PDI-tetraPMMA (DP58), and PDI-tetraPBMA (DP52). The concentration of the polymers was 5.0 μM. The excitation wavelength was 497 nm.

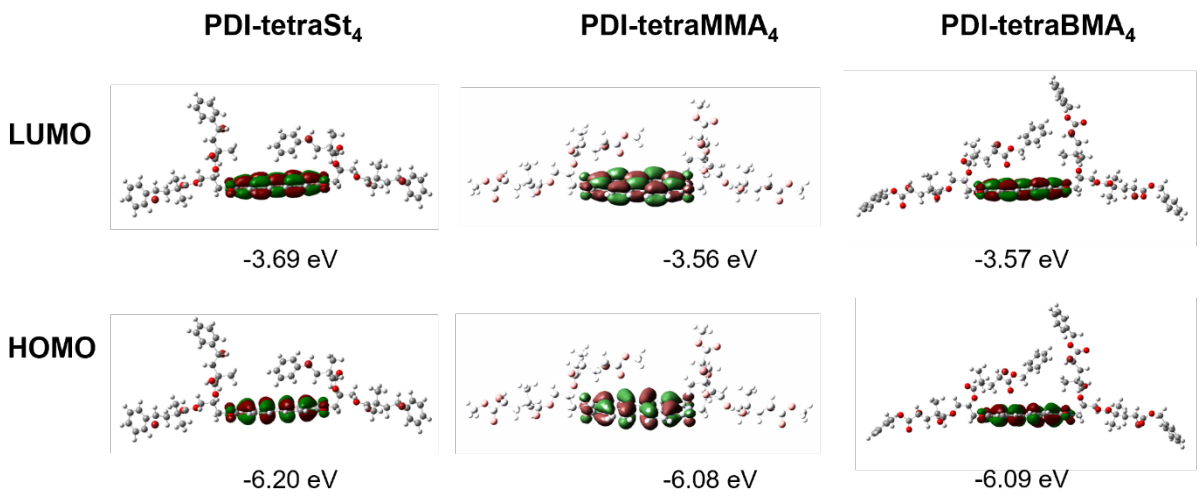

Figure S7. LUMO and HOMO energies and distributions of PDI oligomers.

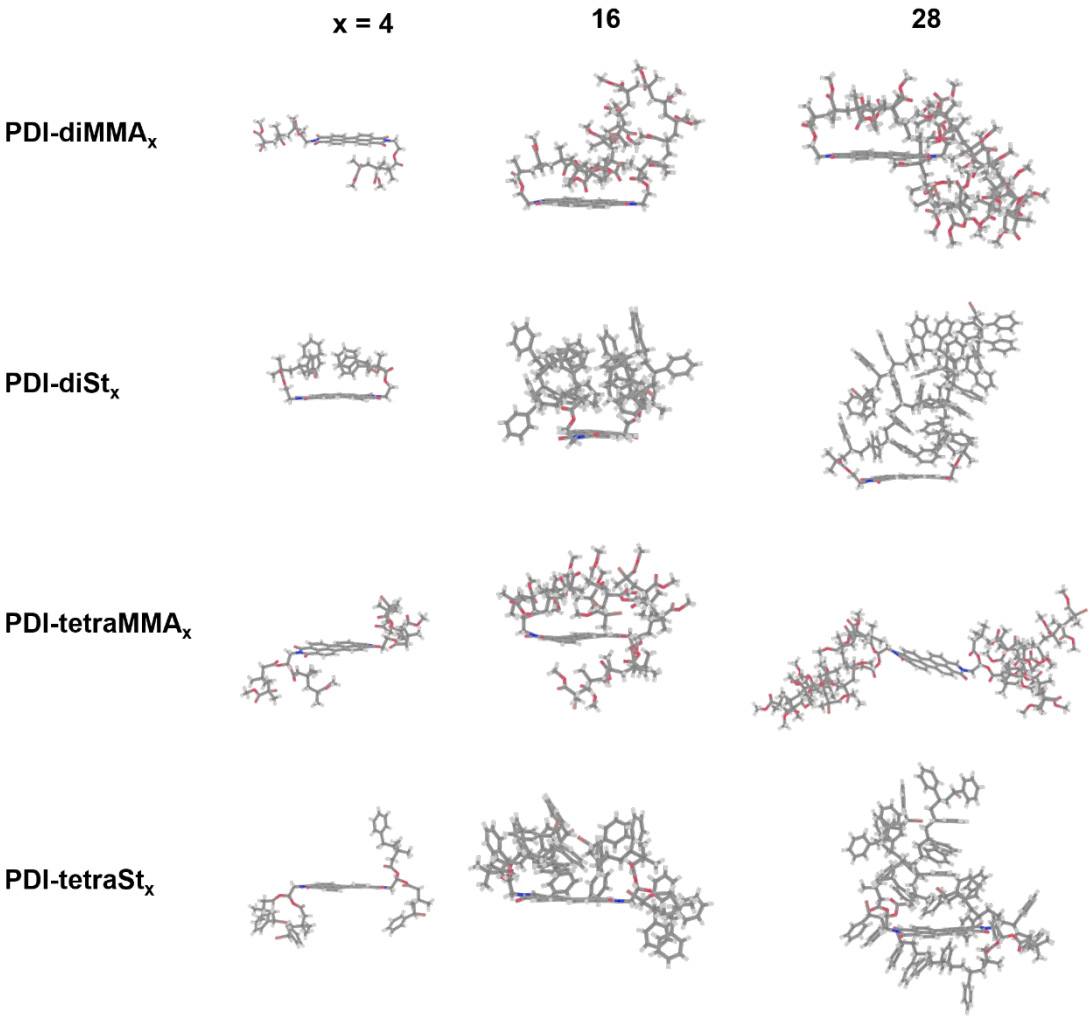

Figure S8. MD simulated oligomer configurations with different monomer and chain length.

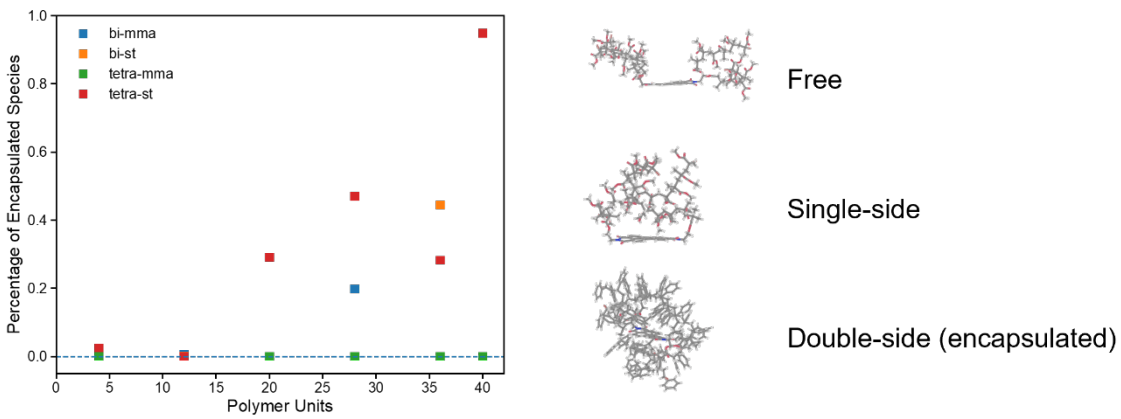

Figure S9. Average percentage of encapsulated PDI core in oligomer configurations with different monomer and chain length.

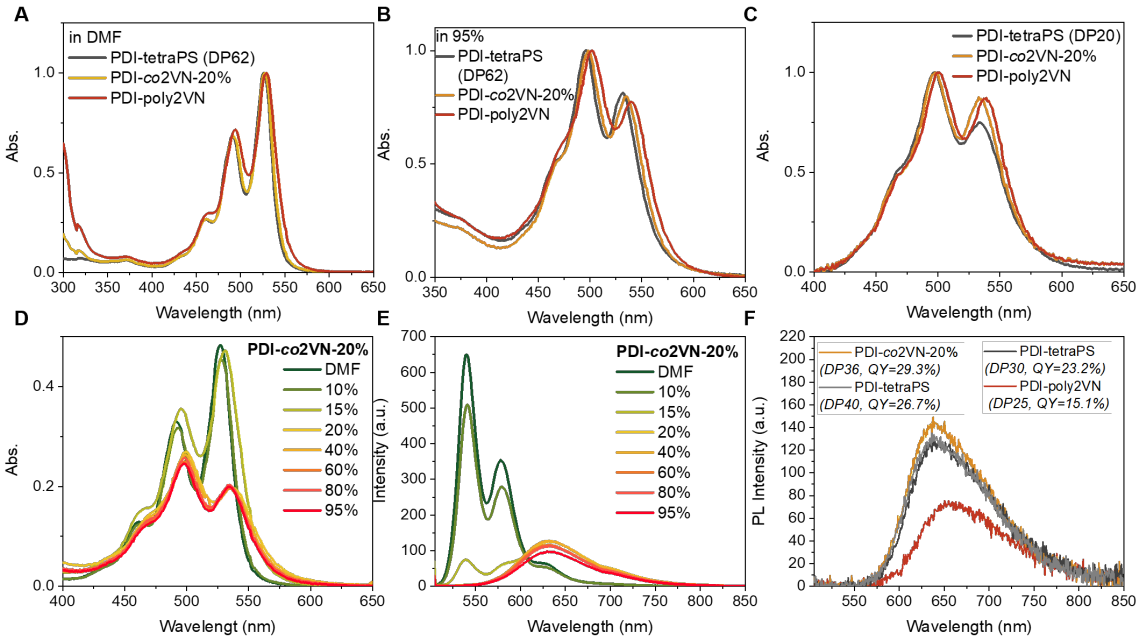

Figure S10. PL properties of PDI-poly2VN and PDI-*co*2VN-20%. (A-C) Comparisons of the absorption spectra of PDI-tetraPS (DP62 in A, B and DP20 in C), PDI-poly2VN, and PDI-*co*2VN-20% in DMF (A), DMF/H_2O (5/95, v/v) (B), or in solid state (C). (D-E) Absorption (D) and PL spectra (E) of PDI-*co*2VN-20% in DMF and DMF/H_2O (90/10 to 5/95, v/v). (F) PL spectra of solid films produced with PDI-tetraPS (DP30 and DP40), PDI-poly2VN, and PDI-*co*2VN-20%. The concentration of the polymers was 5.0 μM. The excitation wavelength was 497 nm.

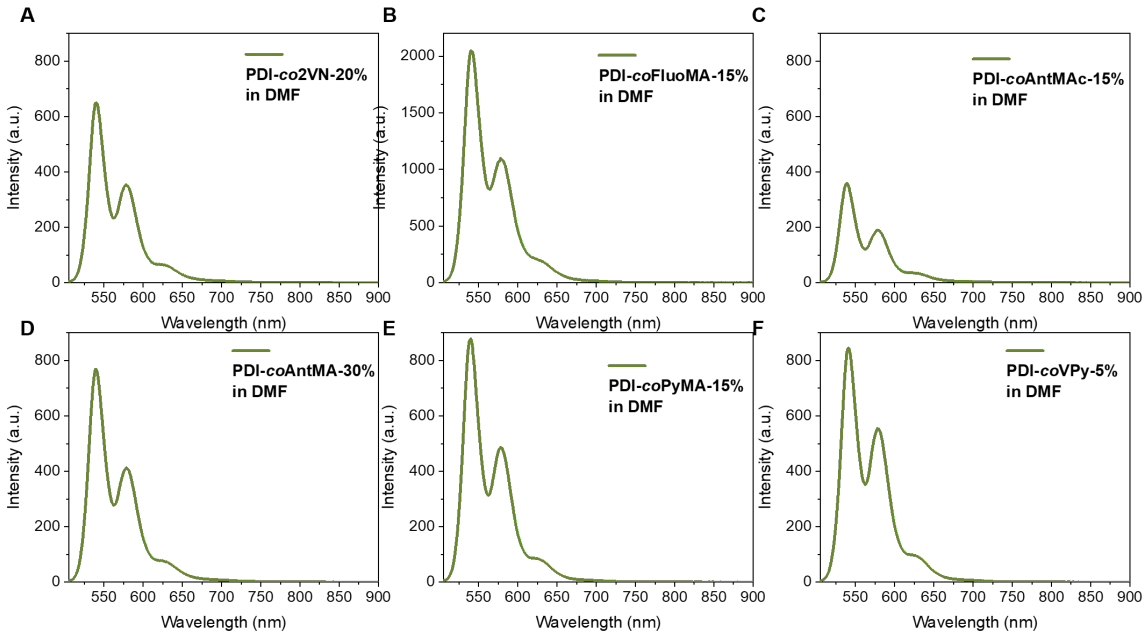

Figure S11. PL properties of PDI copolymers with different PAMs. (A-F) PL spectra of PDI copolymers with different PAMs at their highest feed in DMF. The concentration of the polymers was 5.0 μM. The excitation wavelength was 497 nm.

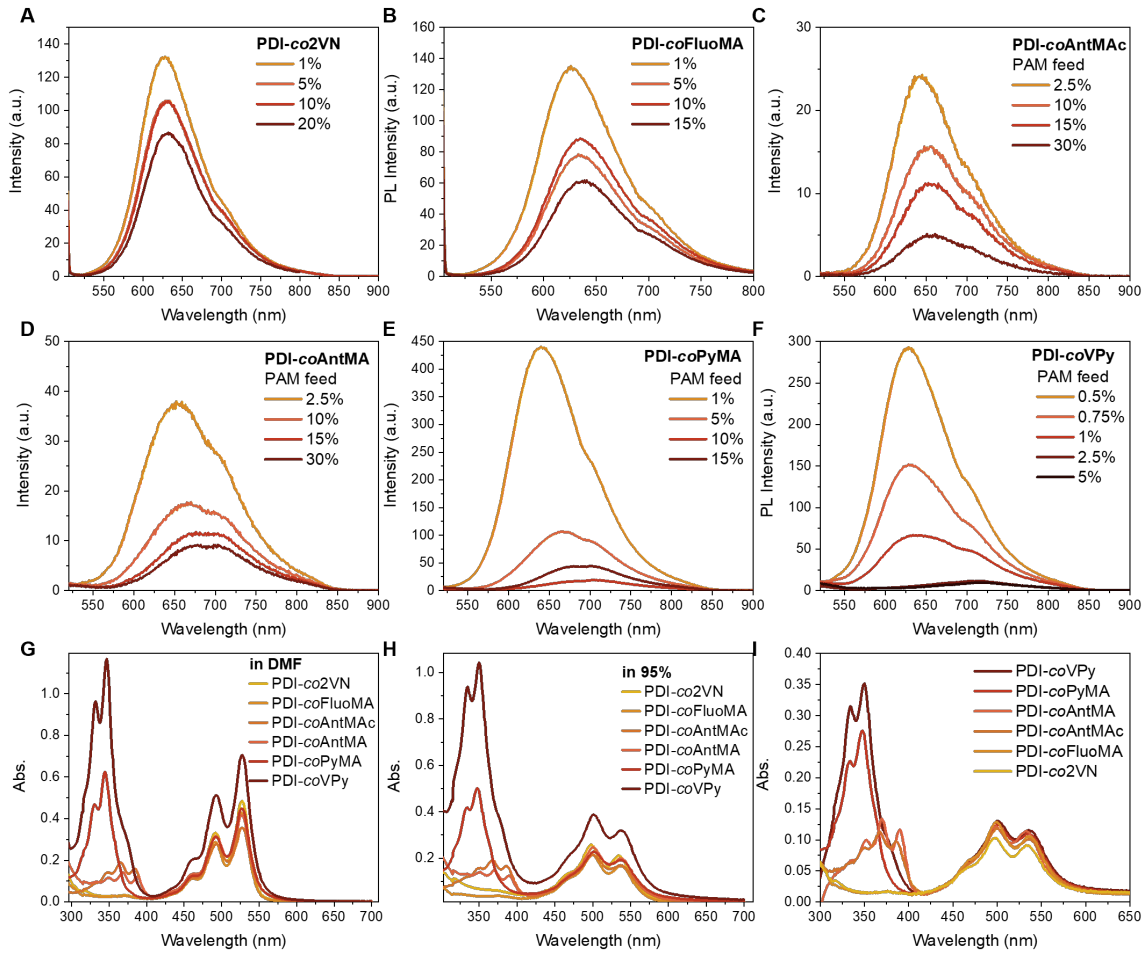

Figure S12. PL properties of PDI copolymers with different PAMs. (A-F) PL spectra of PDI copolymers with different PAMs in DMF/H_2O (5/95, v/v). (G-I) absorption spectra of PDI copolymers with the highest PAM feed in DMF (G), DMF/H_2O (5/95, v/v) (H), or in solid state (I). The concentration of the polymers was 5.0 μM. The excitation wavelength was 497 nm.

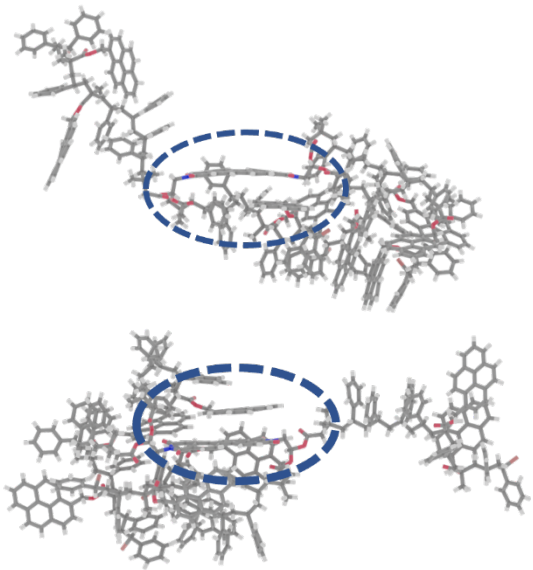

Figure S13. MD stimulated configuration of the copolymer PDI-poly(St_{36}-*co*-VPy_4) in solution. PDI-pyrene pairs were highlighted.

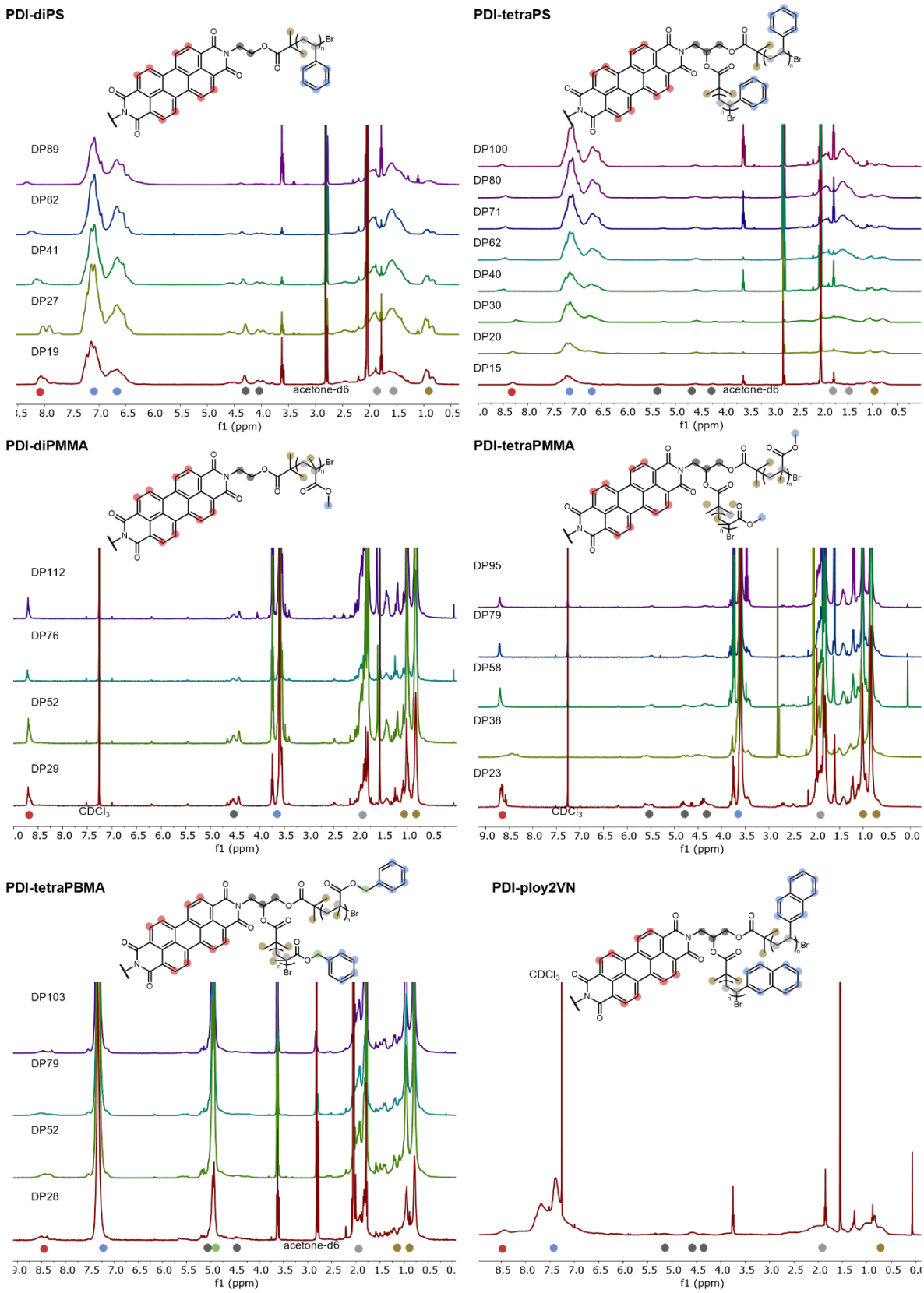

Figure S14. ^{1}H NMR spectra of the PDI homopolymers.

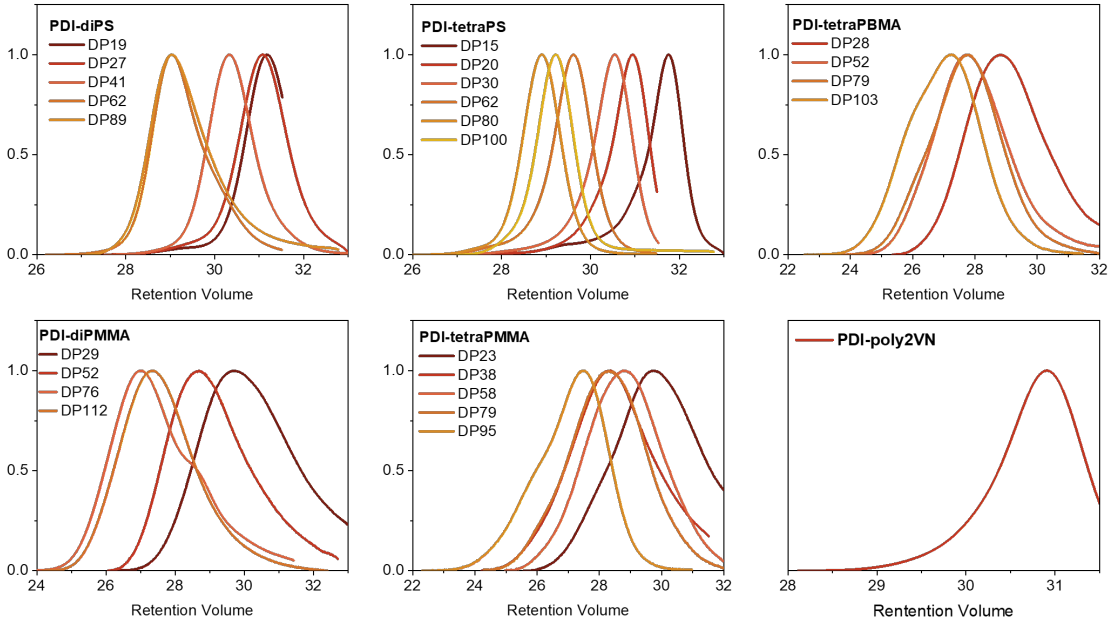

Figure S15. GPC curves of PDI homopolymers with different molecular weights.

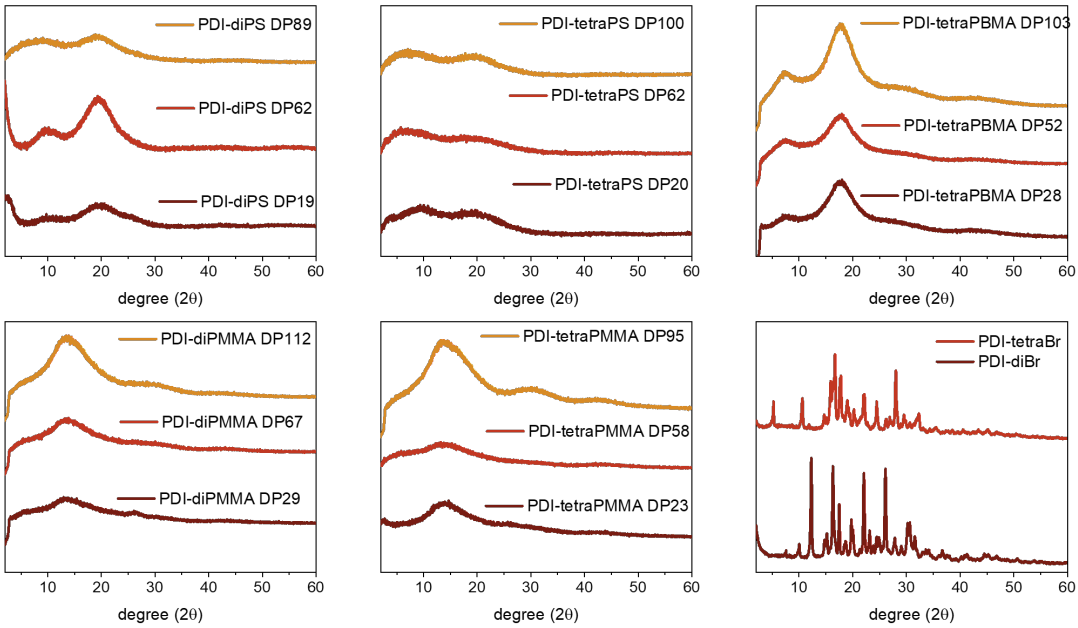

Figure S16. Powder X-ray diffraction patterns of PDI homopolymers with different molecular weights and PDI initiators.

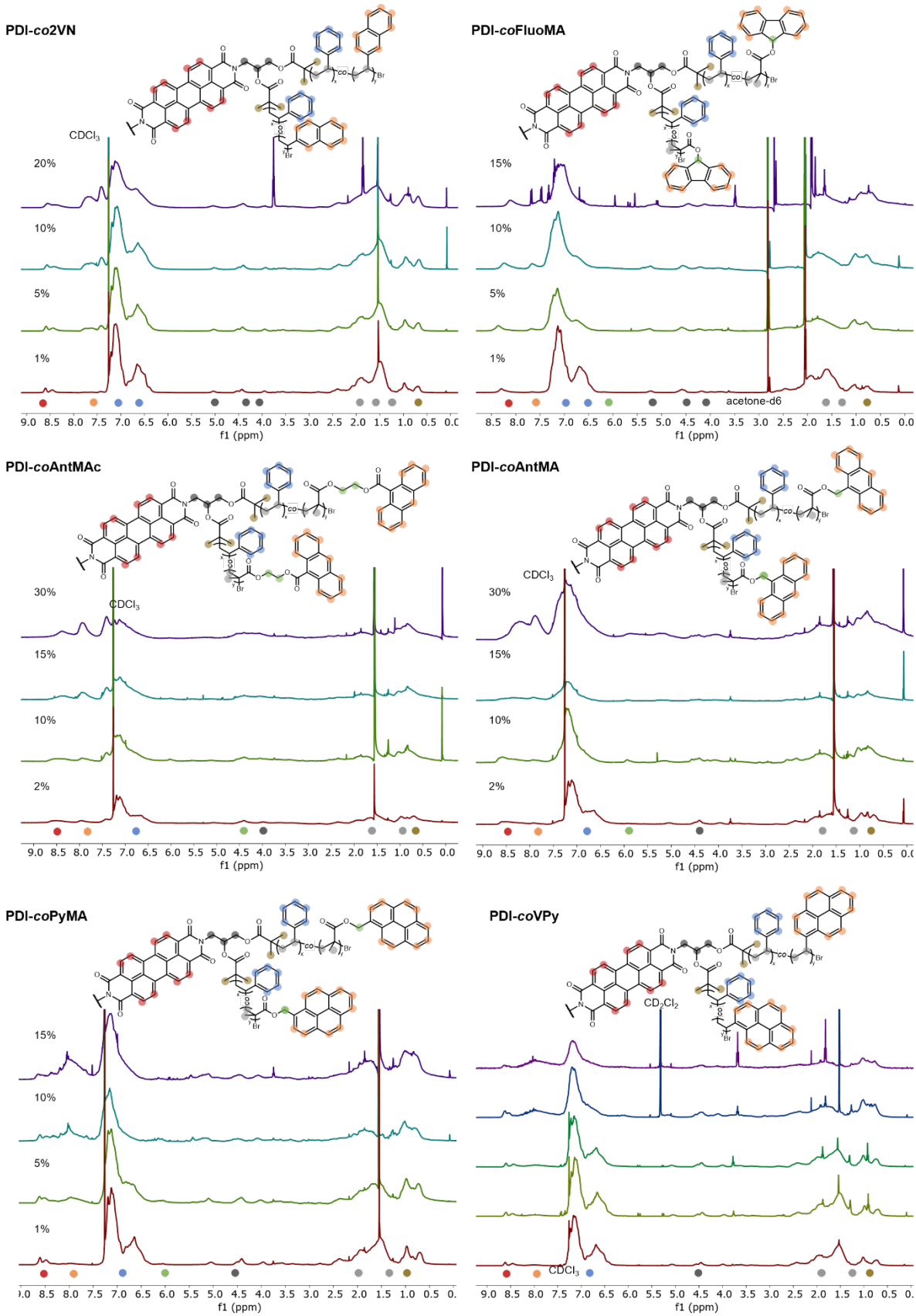

Figure S17. ^{1}H NMR spectra of the PDI copolymers.

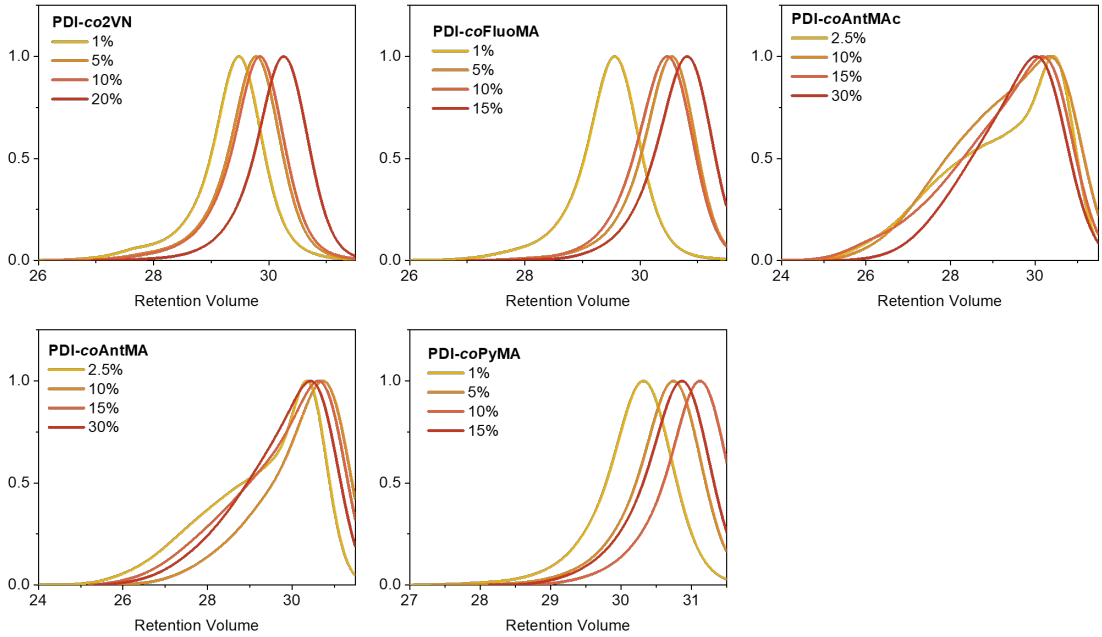

Figure S18. GPC curves of PDI copolymers at various PAM feeds.

Reference

(1) G. Sheldrick, SHELXT - Integrated space-group and crystal-structure determination. Acta Crystallogr. A **2015**, 71, 3–8. DOI: 10.1107/S2053273314026370.

(2) G. Sheldrick, Crystal structure refinement with SHELXL. Acta Crystallogr. C **2015**, 71, 3–8. DOI: 10.1107/S2053229614024218.

(3) O. V. Dolomanov, L. J. Bourhis, R. J. Gildea, J. A. K. Howard, H. Puschmann, OLEX2: A complete structure solution, refinement and analysis program. J. Appl. Crystallogr. **2009**, 42, 339–341. DOI:10.1107/S0021889808042726.

(4) Wohlfarth, Ch. "Dielectric constant of the mixture (1) water;(2) N, N-dimethylformamide: Data extract from Landolt-Börnstein IV/17: Static Dielectric Constants of Pure Liquids and Binary Liquid Mixtures." **2008**, Supplement to IV/6: 550-551.

(5) Aminabhavi, Tejraj M., and Bindu Gopalakrishna. "Density, viscosity, refractive index, and speed of sound in aqueous mixtures of N, N-dimethylformamide, dimethyl sulfoxide, N, N-dimethylacetamide, acetonitrile, ethylene glycol, diethylene glycol, 1, 4-dioxane, tetrahydrofuran, 2-methoxyethanol, and 2-ethoxyethanol at 298.15 K." Journal of Chemical and Engineering Data 40, **1995**, no. 4: 856-861.

(6) Balakrishnan, K.; Datar, A.; Naddo, T.; Huang, J.; Oitker, R.; Yen, M.; Zhao, J.; Zang, L. Effect of Side-Chain Substituents on Self-Assembly of Perylene Diimide Molecules: Morphology Control. *Journal of the American Chemical Society* **2006**, *128* (22), 7390-7398. DOI: 10.1021/ja061810z.

(7) He, Y.; Mao, C.; Duan, M.; Fan, L.; Wang, X.; Cai, Y.; Du, M.; Hu, M.; Hu, P.; Cheng, Q.; et al. Rescuing the solid-state fluorescence of perylene diimide dyes by host–guest isolation. *Organic Chemistry Frontiers* **2022**, *9* (23), 6466-6474. DOI: 10.1039/D2QO01358D.

(8) Ghosh, S.; Li, X.-Q.; Stepanenko, V.; Würthner, F. Control of H- and J-Type π Stacking by Peripheral Alkyl Chains and Self-Sorting Phenomena in Perylene Bisimide Homo- and Heteroaggregates. *Chemistry – A European Journal* **2008**, *14* (36), 11343-11357, https://doi.org/10.1002/chem.200801454..

(9) Lim, J. M.; Kim, P.; Yoon, M.-C.; Sung, J.; Dehm, V.; Chen, Z.; Würthner, F.; Kim, D. Exciton delocalization and dynamics in helical π-stacks of self-assembled perylene bisimides. *Chemical Science* **2013**, *4* (1), 388-397, 10.1039/C2SC21178E. DOI: 10.1039/C2SC21178E.

(10) Chen, Z.; Stepanenko, V.; Dehm, V.; Prins, P.; Siebbeles, L. D. A.; Seibt, J.; Marquetand, P.; Engel, V.; Würthner, F. Photoluminescence and Conductivity of Self-Assembled π–π Stacks of Perylene Bisimide Dyes. *Chemistry – A European Journal* **2007**, *13* (2), 436-449, https://doi.org/10.1002/chem.200600889..

(11) Zhao, H.; Hussain, S.; Liu, X.; Li, S.; Lv, F.; Liu, L.; Wang, S. Design of an Amphiphilic Perylene Diimide for Optical Recognition of Anticancer Drug through a Chirality-Induced Helical Structure. *Chemistry – A European Journal* **2019**, *25* (42), 9834-9839, https://doi.org/10.1002/chem.201901948.

(12) Würthner, F. Perylene bisimide dyes as versatile building blocks for functional supramolecular architectures. *Chemical Communications* **2004**, (14), 1564-1579. DOI: 10.1039/B401630K.